Scientific Research Publishing

Open Journal of Civil Engineering, 2023, 13, 454-478
https://www.scirp.org/journal/ojce
ISSN Online: 2164-3172
ISSN Print: 2164-3164

The Structural Responses of Columns under Various Loadings

Yihong Guo

School of Physics, Faculty of Science, University of New South Wales, Sydney, New South Wales, Australia
Email: cindyt@capstone-research.com

How to cite this paper: Guo, Y.H. (2023) The Structural Responses of Columns under Various Loadings. *Open Journal of Civil Engineering*, **13**, 454-478.
https://doi.org/10.4236/ojce.2023.133034

Received: June 12, 2023
Accepted: September 3, 2023
Published: September 6, 2023

Abstract

This paper focuses on the seismic resistance of one-storied factories, which are commonly used in China due to their flexibility, low cost, and short construction period. With the increasing demand for construction materials, these factories play a vital role in meeting the demands of urbanization and infrastructure development. The seismic resistance of these factories is critical to ensure safety, and this paper presents research on this topic. The paper highlights the advantages of one-storied factories, such as low maintenance cost and seismic resistance, and emphasizes the importance of conducting research on their seismic resistance to ensure safety in construction projects.

Keywords

Structural Design, Infinite Element Analysis, Abaqus, Infrastructure

1. Introduction

The growth of the population leads to a high demand for infrastructure and construction. One solution to meet this demand is the use of one-story factories. These factories not only serve the purpose of construction but can also accomplish a variety of missions such as storage, manufacturing, and power generation. Their effectiveness, feasibility, cost-effectiveness, and safety make them an ideal choice for the fast-paced modern society. The short construction period of one-story factories is another advantage, as it allows for a faster completion of projects and can avoid potential damage from severe weather or delays in work. By utilizing one-story factories, economic benefits can be maximized. Steel structure is utilized throughout the study. Steel is a popular material for constructing one-story buildings due to its numerous properties, some of which are:

1) Strength. Steel is an incredibly strong material, which makes it an ideal

choice for construction purposes. It can support heavy loads and withstand external forces such as wind and earthquakes.

2) Durability. Steel is highly durable and can last for many years without deteriorating. It is resistant to corrosion, rust, and fire, which means that it requires minimal maintenance.

3) Versatility. Steel can be easily fabricated into various shapes and sizes to suit specific building requirements. This makes it a versatile material that can be used for a wide range of construction projects.

4) Cost-effective. Steel is a cost-effective material compared to other building materials such as concrete or wood. It is readily available and requires less labor and time to install, which makes it a popular choice for construction projects.

5) Eco-friendly. Steel is an eco-friendly material as it can be recycled, which reduces the environmental impact of construction. Additionally, the energy required to produce steel is much lower than that of other building materials.

The utilization of steel structures in construction projects has witnessed a remarkable surge owing to their exceptional properties. As a result, extensive researches have been conducted to explore various aspects of steel structures, ranging from their design and fabrication to their performance under different loading conditions.

Li Mengnan (2020) developed a method for identifying the continuous collapse of shell structures based on structural response sensitivity, which enriched the design content of shell structures against continuous collapse and has engineering significance for advancing the development of shell structures. The continuous collapse criterion of shell structures based on strain energy sensitivity was proposed [1].

Peng Shengyue (2021) proposed the optimal layout of double-limb lattice column based on lateral stiffness, the optimal division ratio of column limbs, and the optimal height-to-span ratio of shoulder beams, providing guidance and suggestions for similar engineering design. Finite element analysis software ABAQUS was used to conduct static non-linear analysis of two types of shoulder beams, A and B, which have significantly different safety margins, to explore their stress performance and failure mechanisms. The effect of the height-to-span ratio of shoulder beams on their bearing capacity was analyzed by changing the prototype design of shoulder beam A. The results showed that shoulder beam A complied with the design concept of "strong nodes and weak members" and had sufficient safety margin, while shoulder beam B failed at the nodes before the members, indicating significantly lower safety margin, which should be avoided in similar designs [2].

Gao Xu (2019) analyzed the effects of material nonlinearity on the static stability and resistance to continuous collapse of a large-span single-layer chord-supported shell structure. The results showed that material nonlinearity had a significant impact on the static stability bearing capacity of the structure, while initial defects had a minor influence. Moreover, under non-uniform load distribution

along the short span direction of the structure, the critical load decreased gradually as the ratio of live load to dead load increased. The structure collapsed when the earthquake acceleration amplitude reached 700 gal under the action of the EL-Centro wave. The weak parts of the hybrid structure were located at the transition connection parts of different structural forms [3].

In 2018, Adeline Ng Ling Ying and Hii Wei Hui from the School of Engineering and Science conducted an experimental study on cold-formed thin-walled steel beam-column joints connected by self-tapping screws, investigating the performance of the connections of cold-formed steel joints through a series of tests [4]. The test specimens included hot-rolled channel steel, cold-formed thin-walled C-shaped steel, and self-tapping screws. Two different C-shaped steels and different numbers of self-tapping screws were used in the experiments. The results showed that the moment-rotation characteristics, rotational stiffness, and connection performance varied with different numbers of self-tapping screws. When four screws were used, the connection performed as a fixed connection. However, when eight, ten, and fourteen screws were used, local buckling was observed in the cold-formed thin-walled steel near the connection. The test results of the connections were compared with those based on the Australian standard, and none of the tested connections could achieve the bending capacity of the connected sections.

In 2003, Huang Chuan, Cui Jia, Long Liping, and others from Chongqing University conducted low-cycle reciprocal loading tests on eight full-scale cold-formed thin-walled C-shaped steel beam-column joint specimens, using self-tapping screws for the connection [5] [6]. The specimens were made of Q235 steel, and the study focused on the influence of plate thickness, self-tapping screw diameter, and spacing on the stiffness of the joint, and concluded that the specimens mainly failed in three forms: inclined connection, shear failure of the screw, and tearing of the end plate. The moment-rotation curve obtained from the test showed a nonlinear relationship between the moment and the rotation of the joint. The number of self-tapping screws, the spacing between them, and the thickness of the connecting plate all affected the stiffness and bending capacity of the joint, with the number of screws and plate thickness having a greater impact. Further experimental research is needed to investigate the optimal combination of connection type, screw diameter, and connecting plate thickness.

In the realm of building research, there has been a noticeable trend where a significant amount of attention has been devoted to exploring the effects of altering the interior structure on building properties. Various studies have investigated aspects such as interior design, spatial arrangements, and material selection, recognizing their impact on factors like occupant comfort, functionality, and energy efficiency. However, there appears to be a relative lack of investigation into the fundamental elements of the building's structure, such as the type of columns or beams employed. This apparent research gap suggests the need for further exploration into the basic structural elements to fully grasp their signi-

ficance in optimizing building design and construction practices. By addressing this imbalance, this study has been conducted focusing on the structural response of the steel-structured factory by employing the H-beams. This study aims to provide a better understanding of the structural response of one-story factories under various loads using the finite element program. By analyzing the maximum load capacity of the factory, readers can gain a better understanding of the potential benefits and limitations of one-story factories as a solution for infrastructure and construction demands. Compared to traditional multi-storied factories, one-story factories can be more cost-effective, safer, and easier to maintain. It is also crucial to consider the environmental impact and energy efficiency of one-story factories.

In conclusion, one-story factories can be an efficient and cost-effective solution to meet the demands of infrastructure and construction in a rapidly growing population. The short construction period, effectiveness, feasibility, cost-effectiveness, and safety of one-story factories make them a suitable choice for modern society. This study also provides valuable insights into the structural response of one-story factories under various loads using ABAQUS 2022 software to model the columns and beams. The columns and beams are segmented based on their shape, and loads are applied to evaluate their bending and deformation behavior. Finally, the columns and beams are assembled in accordance with the pre-determined layout.

2. Modeling

2.1. Geometry Design

In this project, ABAQUS 2022 is chosen as the simulation software due to its exceptional capability in modeling various materials. Additionally, Abaqus has a large capacity for structural computation and a wide range of structural modeling functions. It offers various types of model units, material properties, and section selection options, which are ideal for simulating the movement and pressure of a one-story factory. Furthermore, Abaqus also allows for easy modeling and visualization of the dynamic load impact on a factory during an earthquake.

Figure 1 illustrates the layout of the one-story factory. The factory has dimensions of 30 m × 66 m and is composed of 32 columns and 2 beams. The columns are evenly spaced with a distance of 6 m between each, except for the corner columns which have a 0.6 m reduction in the direction of the beam as indicated in the Figure. Additionally, the columns have an extended platform for the crane rail. The columns with numbers are responsible for carrying the crane rail and roof but the columns on the 30 m sides are not load bearing.

As shown in Figure 2, the columns of the one-story factory are initially modeled in ABAQUS with millimeter dimensions. The columns in the original drafting are made of concrete and reinforcement bars, however, for this project,

a pure steel structure is chosen. The properties of the steel structure are chosen in accordance with the Chinese standards. To construct the column, it is divided into four separate parts as illustrated in Figure 3.

The parts of the column are placed together using the assembly function in Abaqus to form a column as shown in Figure 4. This process allows for the accurate representation of the physical column through the assembly of its individual parts. The use of ABAQUS 2022 in this process ensures the proper integration of all components and the ability to accurately simulate the behavior of the column under various loads.

Then the four parts are combined into a whole column using the merge function of ABAQUS. The merging parts in ABAQUS combines the separate parts into a single part, then the column can be considered as an individual now. The top beam which is connecting to the roof is modeled by drawing the cross section and assigning the cross section with a length. For this study, the top beam is not a principal force bearing area, but the rail which runs the crane is. So, the top beam is simplified from the original beam in Figure 5, to the rectangular beam in Figure 6 which has the same length but with a 300 mm × 400 mm rectangular cross section.

The rail that holds the crane is selected from the American standard rail ASCE25. And Figure 7 shows the cross section of the rail from Shanghai Qilang Industrial Co., Ltd. [7].

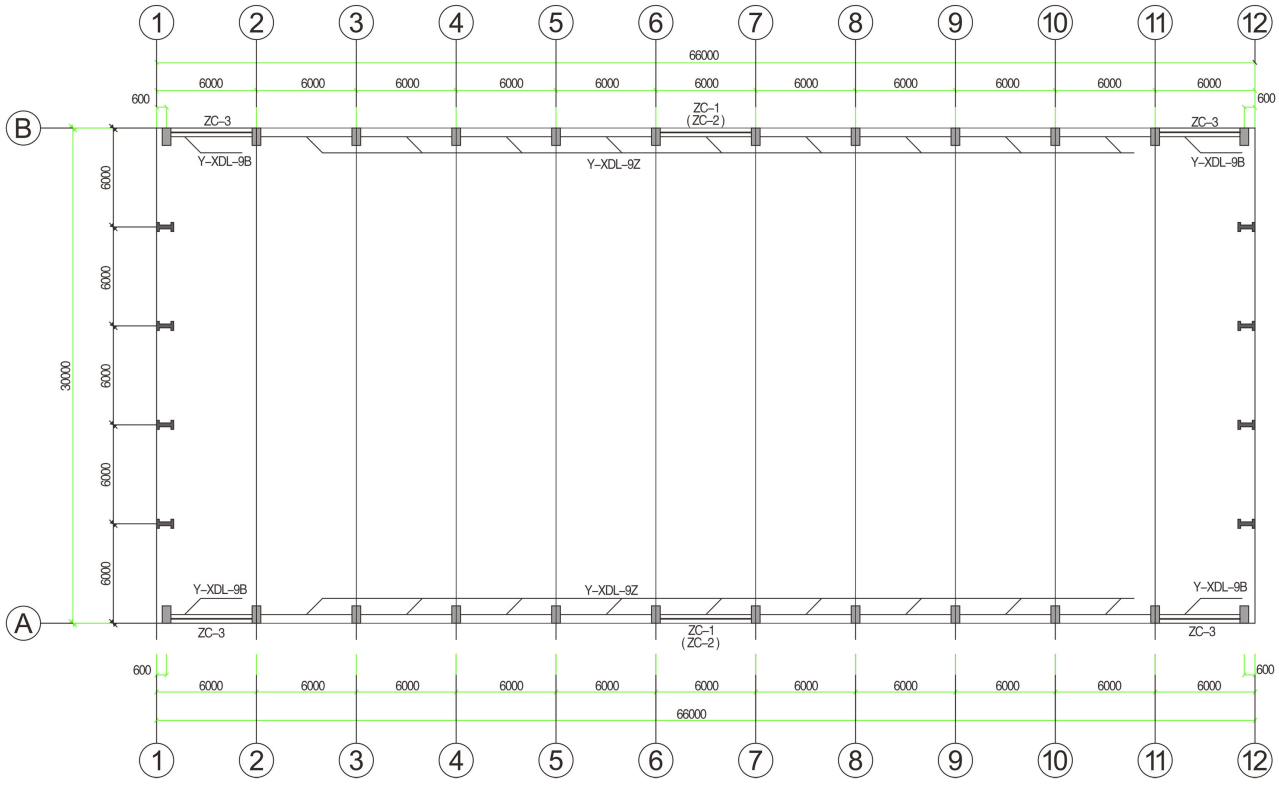

Figure 1. One-storied factory arrangement diagram.

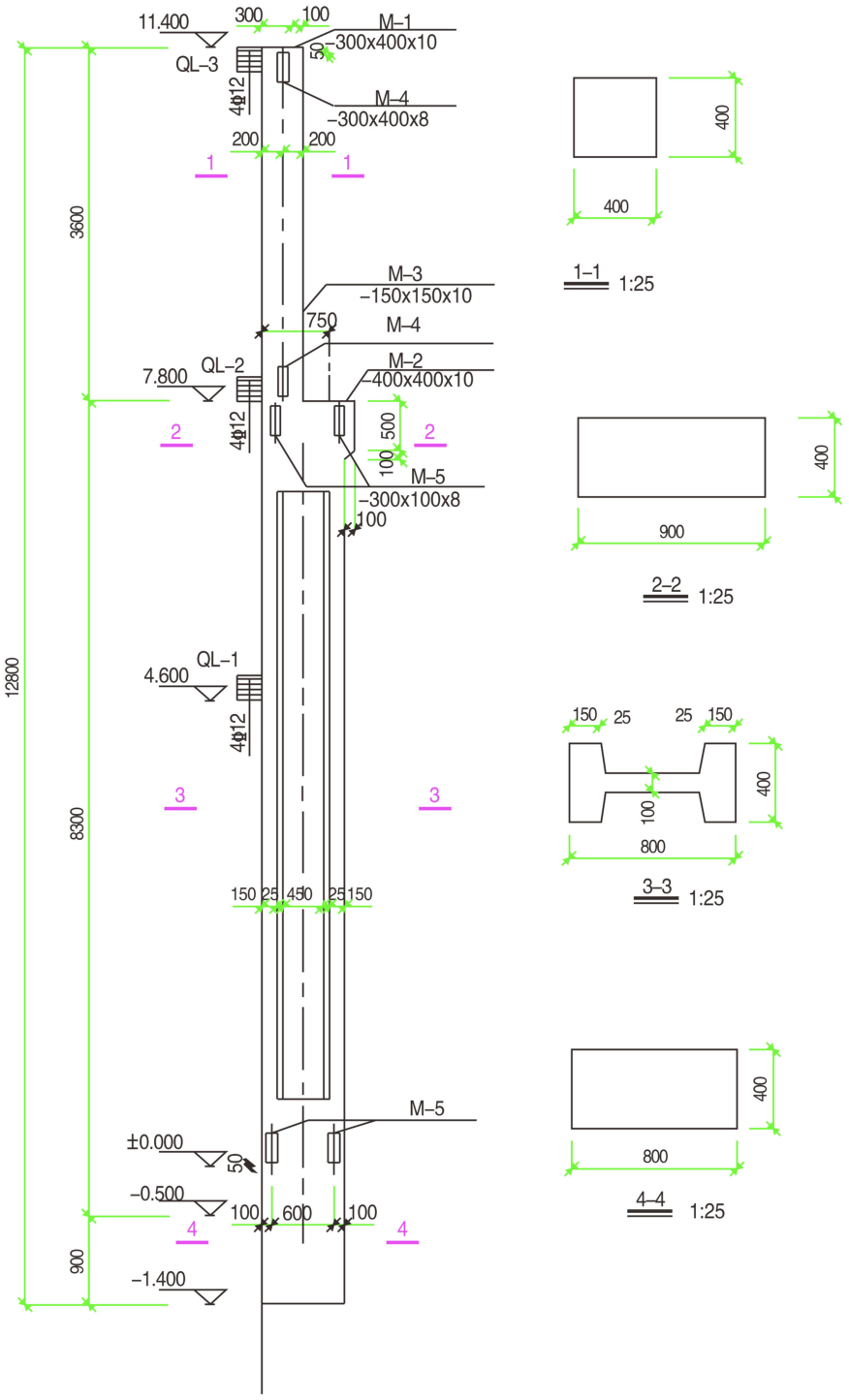

Figure 2. Drafting of the column.

The rail is modeled using Abaqus with the function of creating parts. After selecting the points on the x-y plane, fillet is created between two lines. The fillet is created by entering the radius and selecting the entries near the end of the fillet. And the cross section is in Figure 8. After creating the cross section, a depth of 64,800 mm is assigned to the cross section.

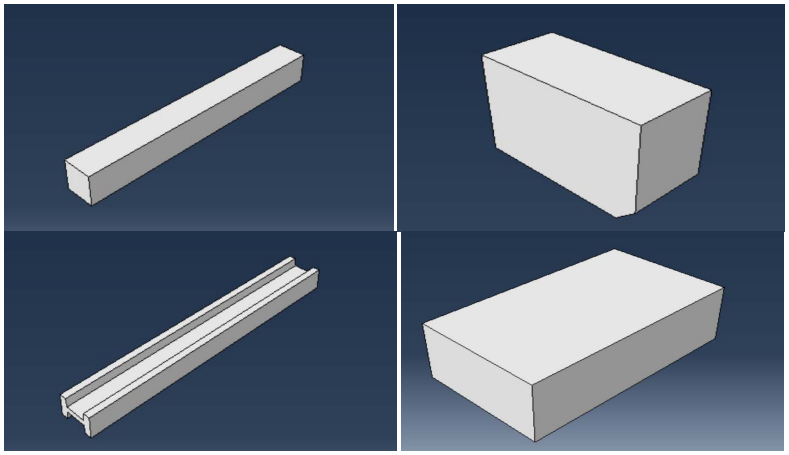

Figure 3. Parts in the model.

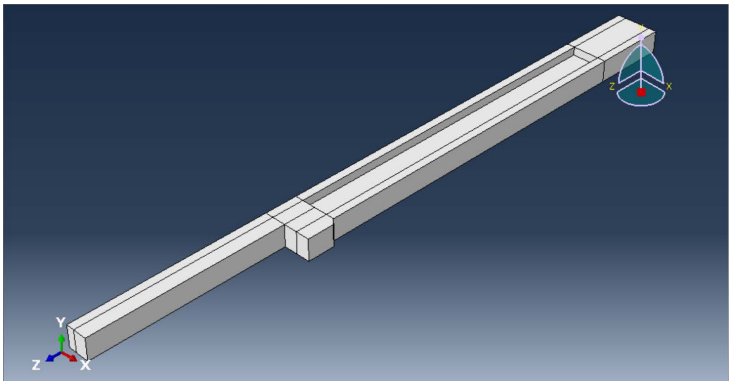

Figure 4. Assembled column.

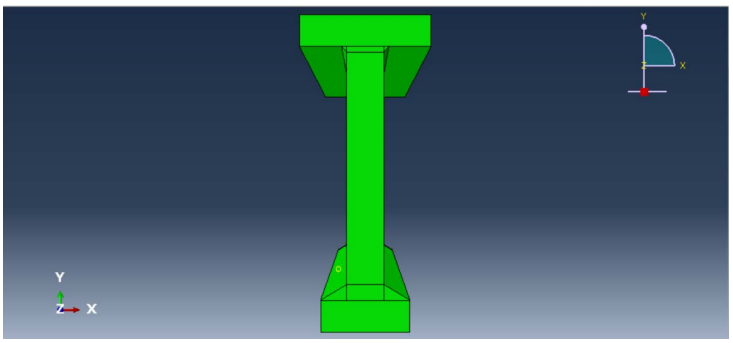

Figure 5. Original beam.

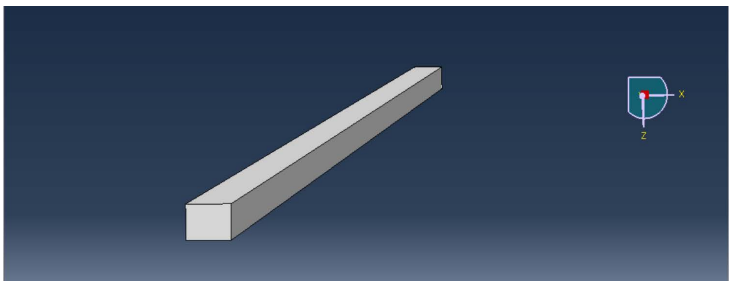

Figure 6. Simplified top beam.

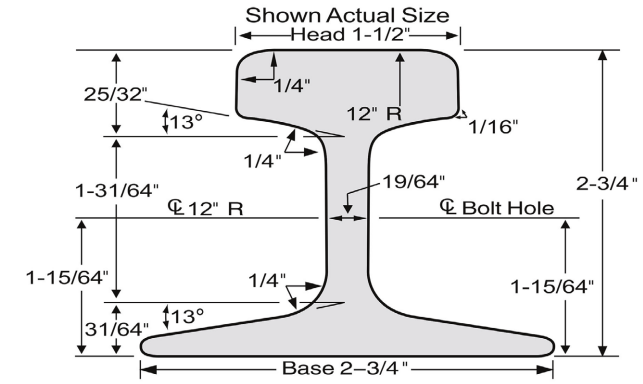

Figure 7. The drafting of the ASCE25 rail.

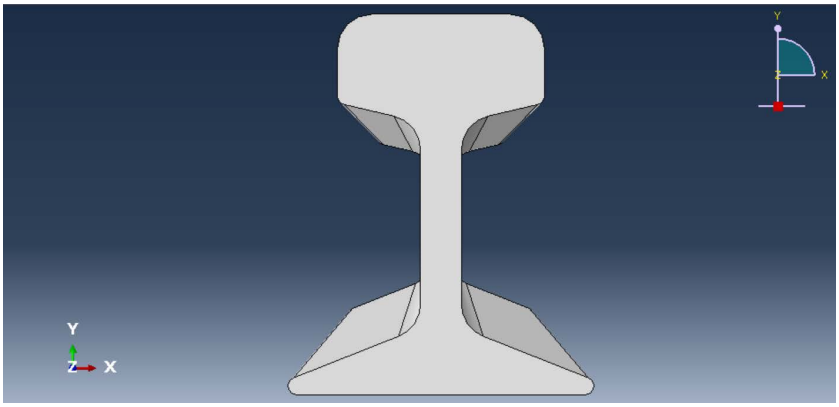

Figure 8. Cross section of the ASCE25 rail.

2.2. Material Properties

2.2.1. Steel

The steel structure is selected for the factory, with density of 7850 kg/m^3 is SI units and 7.85 × 10^{-6} kg/mm^3 in this project's standard. The steel has a Poisson ratio of 0.3, young's modulus of 190,000 N/mm.

2.2.2. Meshing

To mesh the whole column, partition has been made to separate the rectangular parts and the triangular parts, as **Figure 9** and **Figure 10** shows.

The meshing of the column is accomplished firstly by creating partitions of the non-rectangular parts to separate the rectangular and triangular parts, *i.e.*, the second part of **Figure 3**. The partition is created using the point normal method to find the partition plane and cut the column by the partition plane, which is shown in **Figure 10**.

Then, the different partition parts of the column are meshed respectively and the mesh is been done according to the principle as follows:

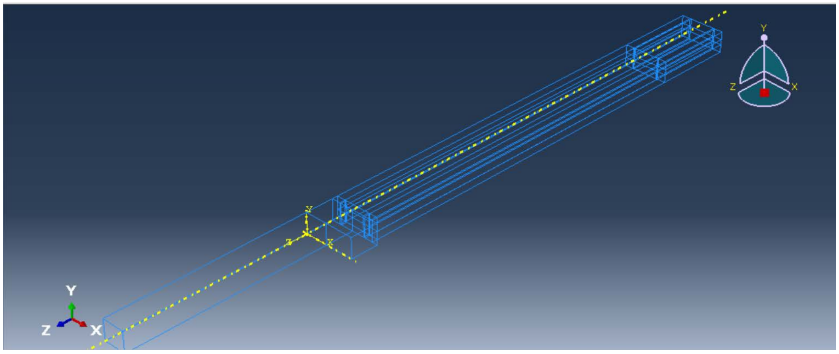

Figure 9. Partition of the column.

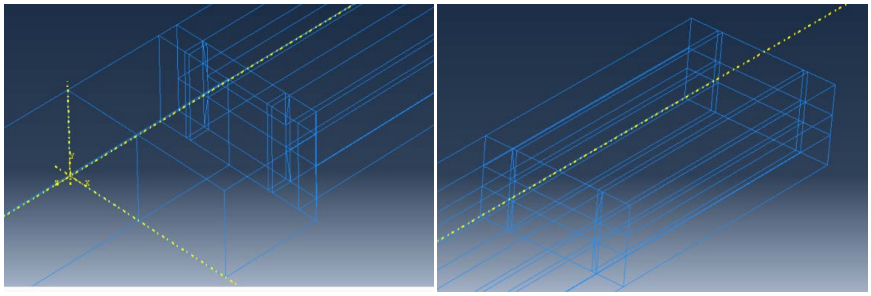

Figure 10. Zoomed in picture of the partition.

1) More element where stress change is high.
2) Less element where stress change is low.
3) No dramatic mesh size, shape change.

After the meshing, the column is ready for simulation as Figure 11 shows.

After being meshed into smaller parts, stress and pressure are assigned on the top of the column and the platform where the crane rail is placed to simulate the loading. Force has been assigned to the platform and the boundary conditions are created at the bottom part where the column connects with the ground to prevent from displacement. The pressure is from a 2000N force in magnitude and downwards in direction and is applied to the whole surface of the platform. The job is then created and submitted for visualization. The visualization is shown in Figure 12.

2.3. Loading

In this section, controlling of variable is used to test the displacement of the column under different loadings, and material properties. The first model is done holding the material property constant. The Poisson ratio is 0.3, the young's modulus is 190,000 N/mm, and the density of steel is 7.85×10^{-6} kg/mm^3. Holding the material property constant, different loads from 0.00418 N/mm^2 to 3.00987 N/mm^2 are assigned respectively to the platform of the column where the crane rail will be placed. Using the JOB function of ABAQUS which will automatically run a full analysis of the structure, it is able to visualize the displacement and stress of the column on different directions, *i.e.*, x-axis, y-axis, and z-axis. Fig-

ures 13-18 show the shaping and stress of column on different directions when there is a loading applied to the platform.

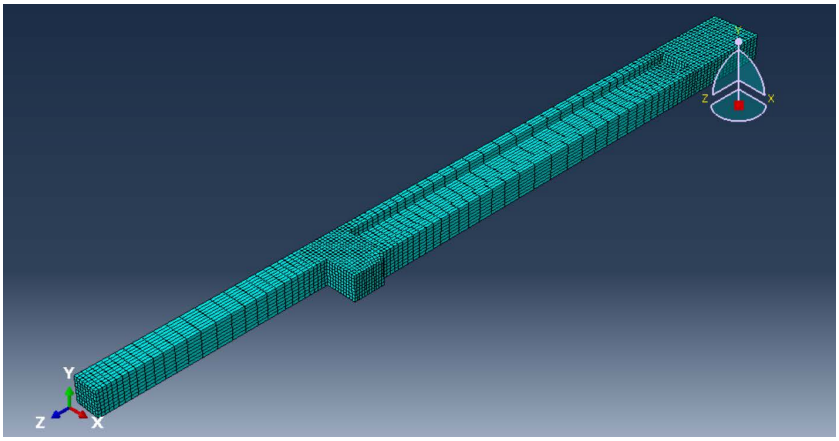

Figure 11. Meshed column.

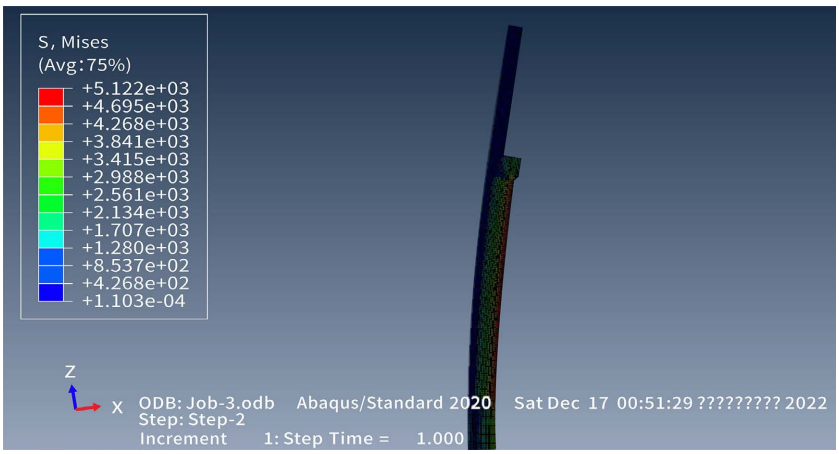

Figure 12. Visualization of the force on the platform.

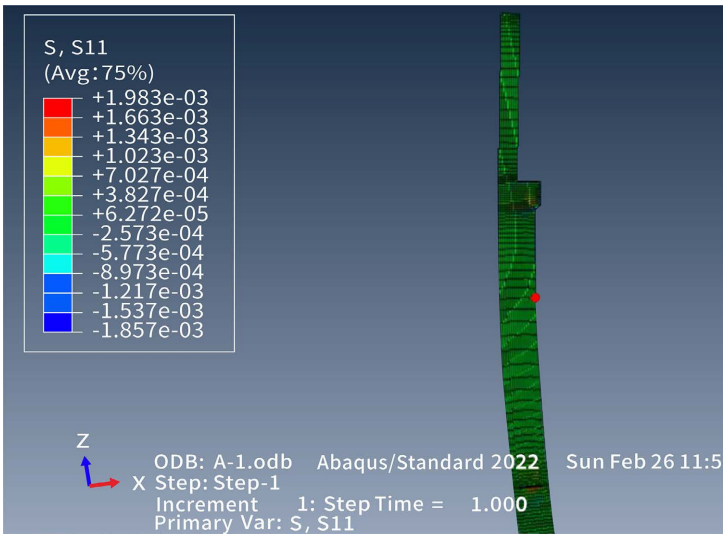

Figure 13. Stress of the column in x direction.

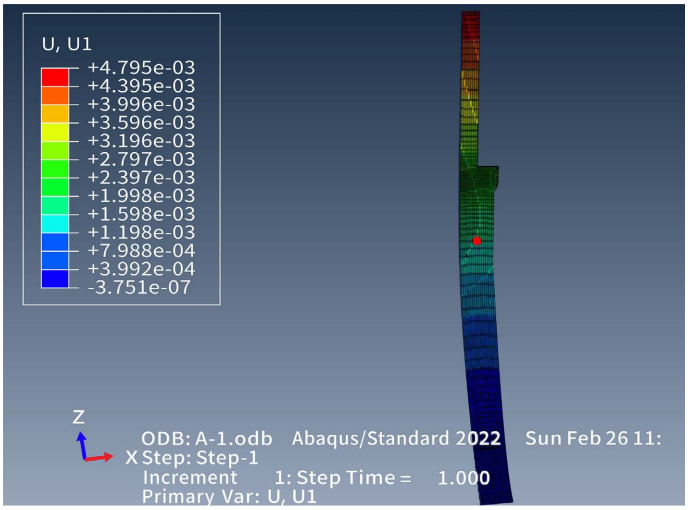

Figure 14. Displacement of the column in x direction.

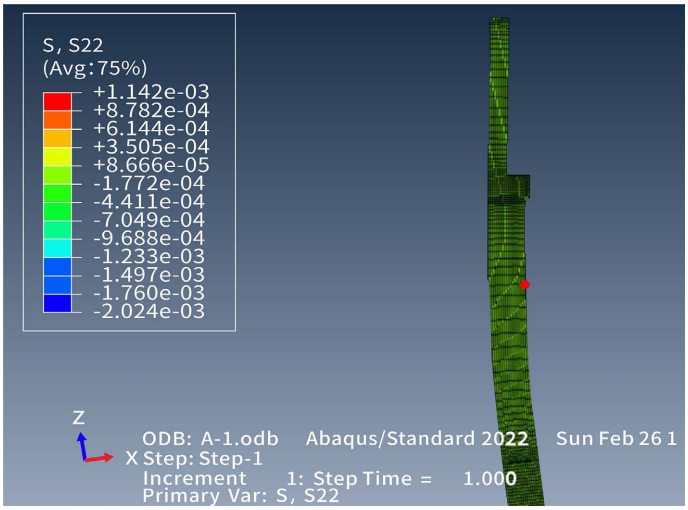

Figure 15. Stress of the column in y direction.

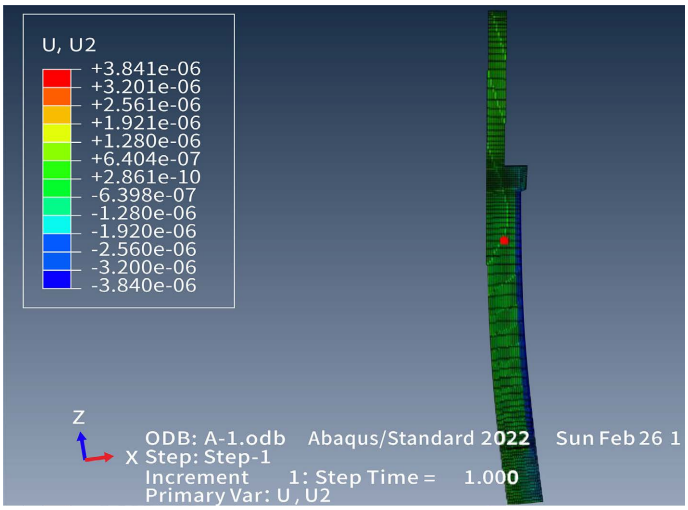

Figure 16. Displacement of the column in y direction.

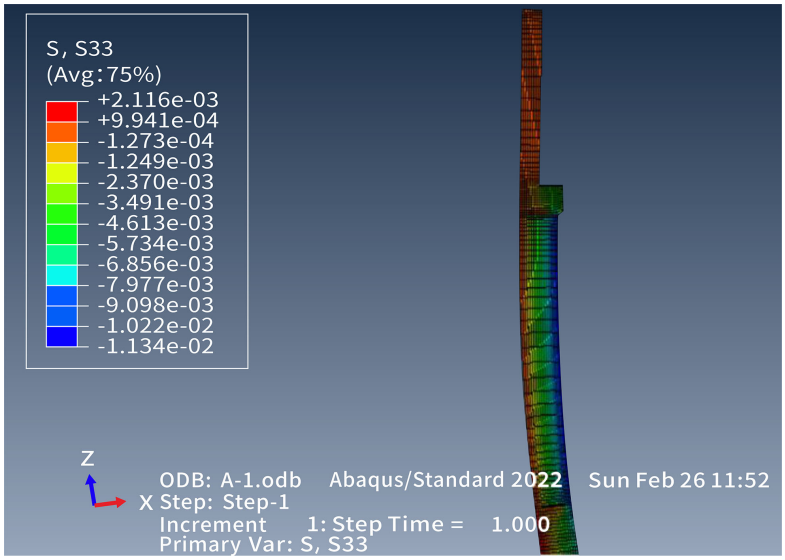

Figure 17. Stress of the column in z direction.

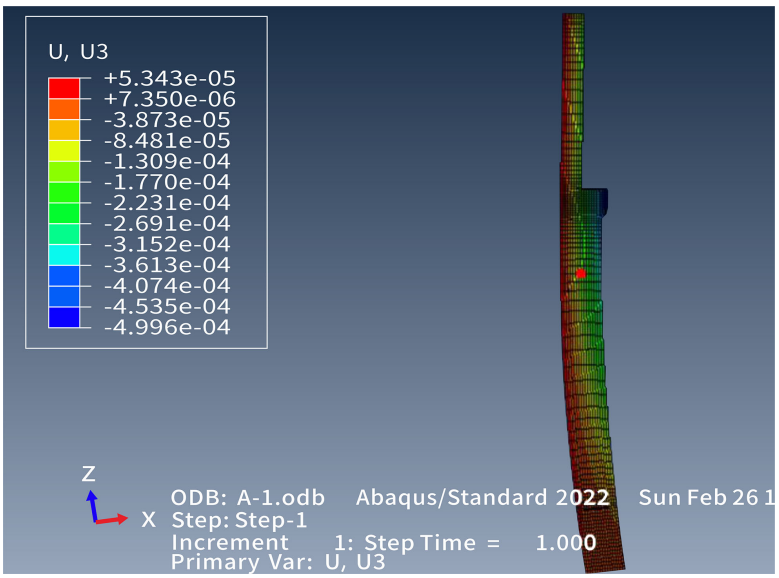

Figure 18. Displacement of the column in z direction.

3. Infinite Element Analysis: ABAQUS

3.1. Load Dependent Measurement

The data are collected after running the job, which is shown in Table 1.

According to Table 1, it is thus able to derive the graphs of displacement versus loading, and stress versus loading. Figure 19 shows the maximum displacement of the column when there is different loading, and Figure 20 shows the minimum displacement of the column.

Upon analyzing the plots depicting the maximum and minimum displacement, it is evident that the displacement occurring along the x-axis is the most distinguishable. Furthermore, the displacement exhibits a linear correlation with

the loading, which is a reasonable observation. As the applied loading increases, the magnitude of the maximum displacement also increases. The plateau observed in the plots implies that the coefficient relating the displacement and pressure remains constant. Conversely, in the y and z directions, the displacement exhibited is comparably lesser than that in the x-direction. The stress-versus-loading plots are presented in Figure 21 and Figure 22, depicting the maximum and minimum stress.

Table 1. Table of displacement and stress on different directions.

loading N/mm^2	U1max mm	U2max mm	U3max mm	S11max N/mm^2	S22max N/mm^2	S33max N/mm^2
0.00418	4.98E−03	3.84E−06	5.34E−05	1.98E−03	1.14E−03	2.12E−03
0.00491	5.63E−03	4.51E−06	6.28E−05	2.33E−03	1.34E−03	2.49E−03
0.00578	6.63E−03	5.31E−06	7.39E−05	2.74E−03	1.58E−03	2.93E−03
0.00680	7.80E−03	6.25E−06	8.69E−05	3.23E−03	1.86E−03	3.44E−03
0.00800	9.18E−03	7.35E−06	1.02E−04	3.80E−03	2.19E−03	4.05E−03
0.00960	1.10E−02	8.82E−06	1.23E−04	4.55E−03	2.62E−03	4.86E−03
0.01152	1.32E−02	1.06E−05	1.47E−04	5.47E−03	3.15E−03	5.83E−03
0.01382	1.59E−02	1.27E−05	1.77E−04	6.56E−03	3.78E−03	6.99E−03
0.01659	1.90E−02	1.52E−05	2.12E−04	7.87E−03	4.53E−03	8.40E−03
0.01991	2.28E−02	1.83E−05	2.55E−04	9.44E−03	5.44E−03	1.01E−02
0.02389	2.74E−02	2.20E−05	3.05E−04	1.13E−02	6.53E−03	1.21E−02
0.52618	6.04E−01	4.84E−04	6.73E−03	2.47E−01	1.44E−01	2.66E−01
0.61904	7.10E−01	5.69E−04	7.91E−03	2.94E−01	1.69E−01	3.13E−01
0.72828	8.35E−01	6.69E−04	9.31E−03	3.46E−01	1.99E−01	3.69E−01
0.85680	9.83E−01	7.87E−04	1.10E−02	4.06E−01	2.34E−01	4.34E−01
1.00800	1.156	9.26E−04	1.29E−02	4.78E−01	2.75E−01	5.10E−01
1.20960	1.388	1.11E−03	1.55E−02	5.74E−01	3.31E−01	6.12E−01
1.45152	1.665	1.33E−03	1.86E−02	6.89E−01	4.00E−01	7.35E−01
1.74182	1.998	1.60E−03	2.23E−02	8.26E−01	4.76E−01	8.82E−01
2.09019	2.398	1.92E−03	2.67E−02	9.92E−01	5.71E−01	1.058
2.50823	2.877	2.31E−03	3.21E−02	1.19	6.85E−01	1.269
3.00987	3.453	2.77E−03	3.85E−02	1.428	8.22E−01	1.523
0.00418	−3.8E−07	−3.8E−06	−0.0005	−0.00186	−0.00202	−0.01134
0.00491	−4.4E−07	−4.5E−06	−0.00059	−0.00218	−0.00238	−0.01332
0.00578	−5.2E−07	−5.3E−06	−0.00069	−0.00257	−0.0028	−0.01568
0.00680	−6.1E−07	−6.2E−06	−0.00081	−0.00302	−0.00329	−0.01845
0.00800	−7.2E−07	−7.4E−06	−0.00096	−0.00356	−0.00387	−0.02171

Continued

0.00960	−8.6E-07	−8.8E-06	−0.00115	−0.00427	−0.00465	−0.02605
0.01152	−1E-06	−1.1E-05	−0.00138	−0.00512	−0.00558	−0.03126
0.01382	−1.2E-06	−1.3E-05	−0.00165	−0.00614	−0.00669	−0.0375
0.01659	−1.5E-06	−1.5E-05	−0.00198	−0.00737	−0.00803	−0.04501
0.01991	−1.8E-06	−1.8E-05	−0.00238	−0.00885	−0.00964	−0.05402
0.02389	−2.1E-06	−2.2E-05	−0.00286	−0.01062	−0.01157	−0.06842
0.52618	−4.7E-05	−0.00048	−0.06288	−0.2338	−0.2548	−1.428
0.61904	−5.6E-05	−0.00057	−0.07398	−0.2751	−0.2998	−1.68
0.72828	−6.5E-05	−0.00067	−0.08704	−0.3236	−0.3527	−1.976
0.85680	−7.7E-05	−0.00079	−0.1024	−0.3807	−0.4149	−2.325
1.00800	−9E-05	−0.00093	−0.1205	−0.4479	−0.4881	−2.735
1.20960	−0.00011	−0.00111	−0.1446	−0.5375	−0.5858	−3.282
1.45152	−0.00013	−0.00133	−0.1736	−0.645	−0.7029	−3.938
1.74182	−0.00016	−0.0016	−0.2082	−0.7741	−0.8437	−4.727
2.09019	−0.00019	−0.00192	−0.2498	−0.9288	−1.012	−5.671
2.50823	−0.00023	−0.0023	−0.2998	−1.115	−1.215	−6.805
3.00987	−0.00027	−0.00277	−0.3597	−1.337	−1.458	−8.166

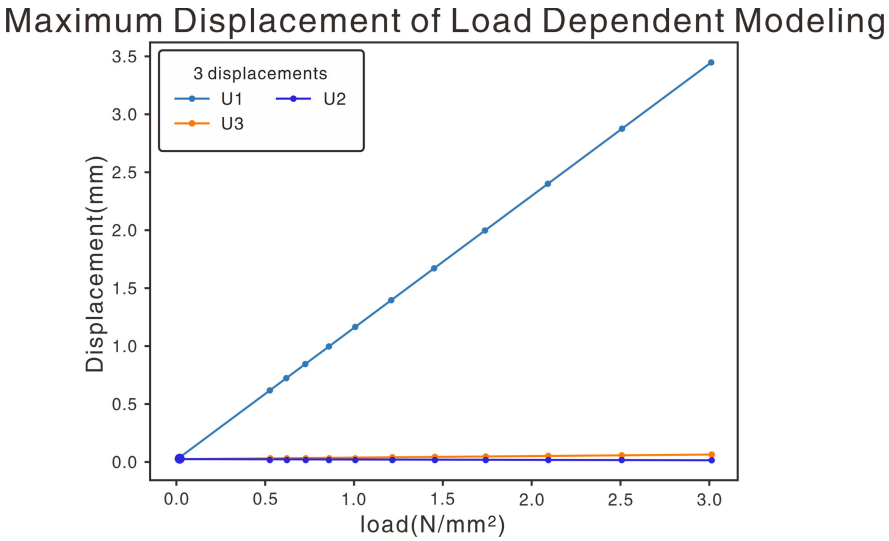

Figure 19. Maximum displacement of column in loading dependent modeling.

Based on the stress plots, it can be observed that there exists a linear relationship between the applied load and the resulting stress. Specifically, as the magnitude of the loading increases, the magnitude of the stress also increases proportionally. Moreover, it is noteworthy that the direction in which the stress exhibits the steepest slope is along the z-axis.

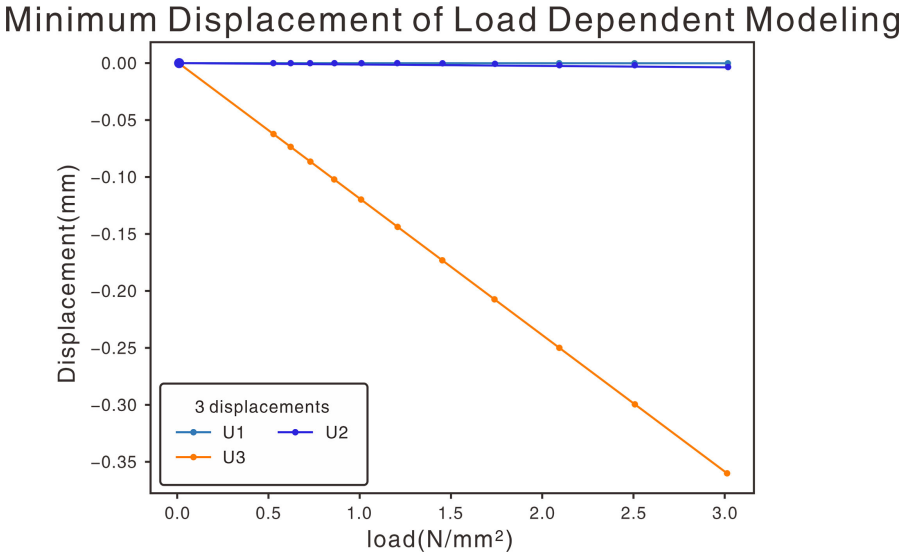

Figure 20. Minimum displacement of column in loading dependent modeling.

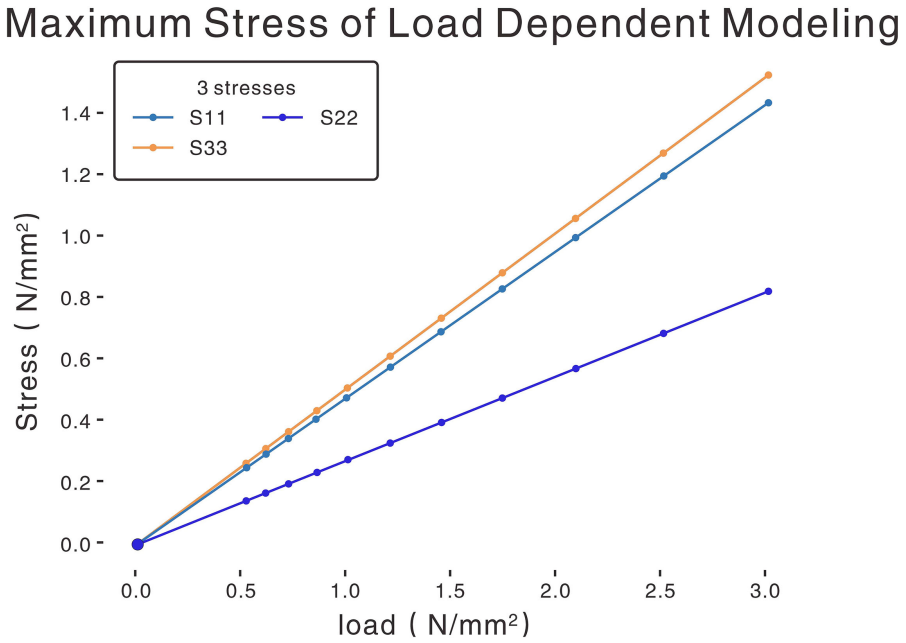

Figure 21. Maximum stress of column in loading dependent modeling.

3.2. Young's Modulus Dependent Measurement

In the second part of this section, a modeling approach dependent on the Young's modulus is performed, utilizing the same material setup as before. The loading is set to a fixed value of 0.008 N/mm^2, as illustrated in the data Tables presented in **Table 2** and **Table 3**.

Utilizing the data provided in the aforementioned Tables, it is possible to establish a correlation between the Young's modulus and the corresponding displacement. It should be noted that under constant loading applied to the platform, the stress experienced by the column in all directions remains constant.

Consequently, the graph of stress and Young's modulus can be disregarded. The plots illustrating the maximum and minimum displacement are presented in Figure 23 and Figure 24, respectively.

Table 2. Table of material property.

Young's modulus N/mm	Poisson's ratio	density (kg/mm^3)	loading N/mm^2
191,500	0.30	7.85E−06	0.00800
193,000	0.30	7.85E−06	0.00800
194,500	0.30	7.85E−06	0.00800
196,000	0.30	7.85E−06	0.00800
197,500	0.30	7.85E−06	0.00800
199,000	0.30	7.85E−06	0.00800
200,500	0.30	7.85E−06	0.00800
202,000	0.30	7.85E−06	0.00800
203,500	0.30	7.85E−06	0.00800
205,000	0.30	7.85E−06	0.00800
206,500	0.30	7.85E−06	0.00800
208,000	0.30	7.85E−06	0.00800
209,500	0.30	7.85E−06	0.00800
211,000	0.30	7.85E−06	0.00800
212,500	0.30	7.85E−06	0.00800
214,000	0.30	7.85E−06	0.00800
215,500	0.30	7.85E−06	0.00800
217,000	0.30	7.85E−06	0.00800
218,500	0.30	7.85E−06	0.00800
220,000	0.30	7.85E−06	0.00800
221,500	0.30	7.85E−06	0.00800
223,000	0.30	7.85E−06	0.00800
224,500	0.20	7.85E−06	0.00800

The information the graphs convey in the chart is that the larger the young's modulus, the smaller the displacement. From the graphs, the maximum displacement in x direction is distinguishable compared to that in the other directions, and it shows linear correlation with the young's modulus. The slope of the line is constant, which means that the coefficient between the displacement and young's modulus is constant.

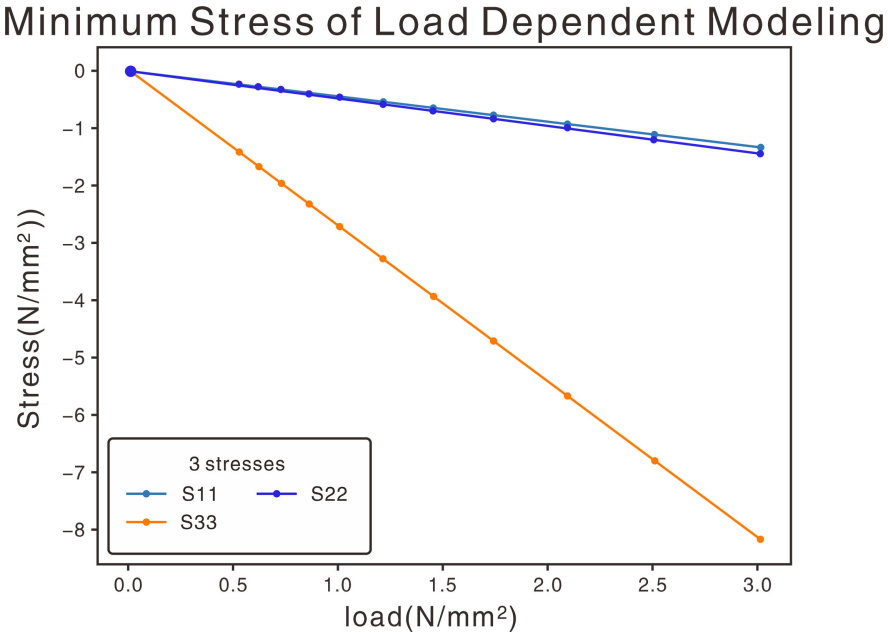

Figure 22. Minimum stress of column in loading dependent modeling.

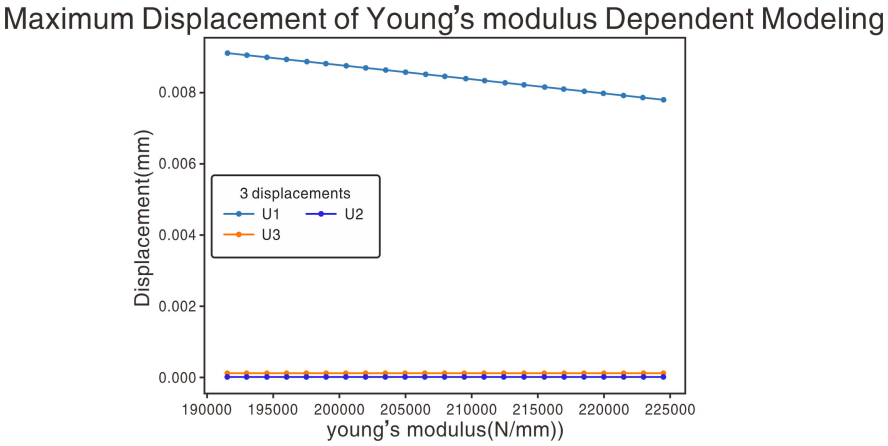

Figure 23. Maximum displacement of young's modulus dependent modeling.

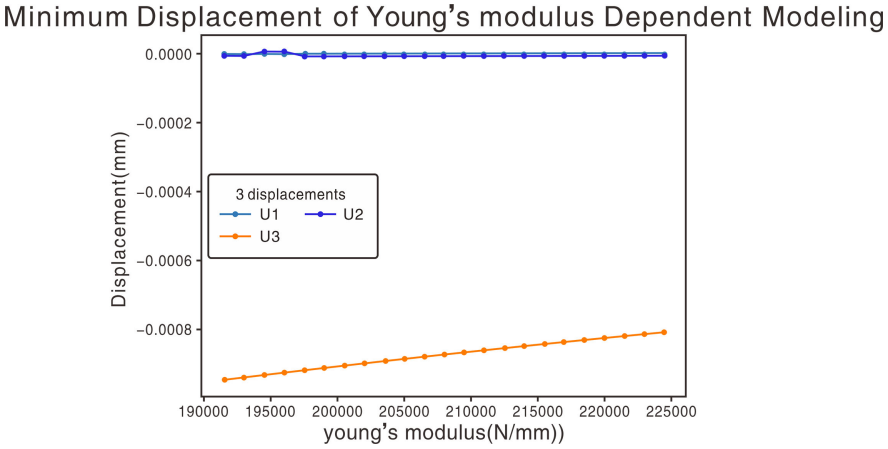

Figure 24. Minimum displacement of young's modulus dependent modeling.

Table 3. Table of displacements and stresses.

U1 max mm	U1min mm	U2max mm	U2min mm	U3max mm	U3min mm	S11 max N/mm²	S11 min N/mm²	S22 max N/mm²	S22 min N/mm²	S33 max N/mm²	S33 min N/mm²
9.11E−03	−7.12E−07	7.29E−06	−7.29E−06	1.11E−04	−9.49E−04	3.80E−03	−3.56E−03	2.19E−03	−3.87E−03	4.05E−03	−2.17E−02
9.03E−03	−7.07E−07	7.24E−06	−7.24E−06	1.01E−04	−9.41E−04	3.80E−03	−3.56E−03	2.19E−03	−3.87E−03	4.05E−03	−2.17E−02
8.96E−03	−7.01E−07	7.18E−06	7.18E−06	9.99E−05	−9.34E−04	3.80E−03	−3.56E−03	2.19E−03	−3.87E−03	4.05E−03	−2.17E−02
8.90E−03	−6.96E−07	7.13E−06	7.13E−06	9.91E−05	−9.27E−04	3.80E−03	−3.56E−03	2.19E−03	−3.87E−03	4.05E−03	−2.17E−02
8.83E−03	−6.91E−07	7.07E−06	−7.07E−06	9.84E−05	−9.20E−04	3.80E−03	−3.56E−03	2.19E−03	−3.87E−03	4.05E−03	−2.17E−02
8.76E−03	−6.86E−07	7.02E−06	−7.02E−06	9.76E−05	−9.13E−04	3.80E−03	−3.56E−03	2.19E−03	−3.87E−03	4.05E−03	−2.17E−02
8.70E−03	−6.80E−07	6.97E−06	−6.97E−06	9.69E−05	−9.06E−04	3.80E−03	−3.56E−03	2.19E−03	−3.87E−03	4.05E−03	−2.17E−02
8.63E−03	−6.75E−07	6.91E−06	−6.91E−06	9.62E−05	−8.99E−04	3.80E−03	−3.56E−03	2.19E−03	−3.87E−03	4.05E−03	−2.17E−02
8.57E−03	−6.70E−07	6.86E−06	−6.86E−06	9.55E−05	−8.93E−04	3.80E−03	−3.56E−03	2.19E−03	−3.87E−03	4.05E−03	−2.17E−02
8.51E−03	−6.65E−07	6.81E−06	−6.81E−06	9.48E−05	−8.86E−04	3.80E−03	−3.56E−03	2.19E−03	−3.87E−03	4.05E−03	−2.17E−02
8.44E−03	−6.61E−07	6.76E−06	−6.76E−06	9.41E−05	−8.80E−04	3.80E−03	−3.56E−03	2.19E−03	−3.87E−03	4.05E−03	−2.17E−02
8.38E−03	−6.56E−07	6.72E−06	−6.71E−06	9.34E−05	−8.73E−04	3.80E−03	−3.56E−03	2.19E−03	−3.87E−03	4.05E−03	−2.17E−02
8.32E−03	−6.51E−07	6.67E−06	−6.67E−06	9.27E−05	−8.67E−04	3.80E−03	−3.56E−03	2.19E−03	−3.87E−03	4.05E−03	−2.17E−02
8.26E−03	−6.47E−07	6.62E−06	−6.62E−06	9.21E−05	−8.61E−04	3.80E−03	−3.56E−03	2.19E−03	−3.87E−03	4.05E−03	−2.17E−02
8.21E−03	−6.42E−07	6.57E−06	−6.57E−06	9.14E−05	−8.55E−04	3.80E−03	−3.56E−03	2.19E−03	−3.87E−03	4.05E−03	−2.17E−02
8.15E−03	−6.38E−07	6.53E−06	−6.53E−06	9.08E−05	−8.49E−04	3.80E−03	−3.56E−03	2.19E−03	−3.87E−03	4.05E−03	−2.17E−02
8.09E−03	−6.33E−07	6.48E−06	−6.48E−06	9.02E−05	−8.43E−04	3.80E−03	−3.56E−03	2.19E−03	−3.87E−03	4.05E−03	−2.17E−02
8.04E−03	−6.29E−07	6.44E−06	−6.44E−06	8.95E−05	−8.37E−04	3.80E−03	−3.56E−03	2.19E−03	−3.87E−03	4.05E−03	−2.17E−02
7.98E−03	−6.24E−07	6.39E−06	−6.39E−06	8.89E−05	−8.31E−04	3.80E−03	−3.56E−03	2.19E−03	−3.87E−03	4.05E−03	−2.17E−02
7.93E−03	−6.20E−07	6.35E−06	−6.35E−06	8.83E−05	−8.26E−04	3.80E−03	−3.56E−03	2.19E−03	−3.87E−03	4.05E−03	−2.17E−02
7.87E−03	−6.16E−07	6.31E−06	−6.31E−06	8.77E−05	−8.20E−04	3.80E−03	−3.56E−03	2.19E−03	−3.87E−03	4.05E−03	−2.17E−02
7.82E−03	−6.12E−07	6.26E−06	−6.26E−06	8.71E−05	−8.15E−04	3.80E−03	−3.56E−03	2.19E−03	−3.87E−03	4.05E−03	−2.17E−02
7.77E−03	−6.08E−07	6.22E−06	−6.22E−06	8.66E−05	−8.09E−04	3.80E−03	−3.56E−03	2.19E−03	−3.87E−03	4.05E−03	−2.17E−02

3.3. Poisson Ratio Dependent Measurement

The third part of this section analyzes the correlation between displacement, stress and Poisson ratio. In this process of modeling, the material properties are holding constant except for the Poisson ratio. The data are shown in Table 4 and Table 5.

From the Tables, the graph showing the relation between Poisson ratio and displacement or the relation between Poisson ratio and the stress can be visualized using the line chart in Figure 25 to Figure 26.

The constancy of displacement in response to a change in Poisson ratio can be attributed to the fact that displacement is dependent on the applied load, whereas Poisson ratio affects the material's ability to deform in response to the load. In this particular measurement, the load is held constant, leading to constant

displacement throughout. The graphical outcome is shown in Figure 27. Furthermore, the magnitude of the displacement is relatively small even when compared to 1 mm.

In an experiment where the load is held constant, changes in Poisson ratio result in slight variations in stress, particularly in the z-direction, and in the x and y directions, the magnitude of stress change is relatively small. From the plot more an increase stress occurred in y direction which corresponds to the longitudinal axis of the column.

Table 4. Material property set up.

No.	Young's modulus N/mm	Poisson's ratio	density (kg/mm^3)	loading N/mm^2
46	200,500	0.25	7.85E−06	0.00800
47	200,500	0.30	7.85E−06	0.00800
48	200,500	0.35	7.85E−06	0.00800
49	200,500	0.40	7.85E−06	0.00800

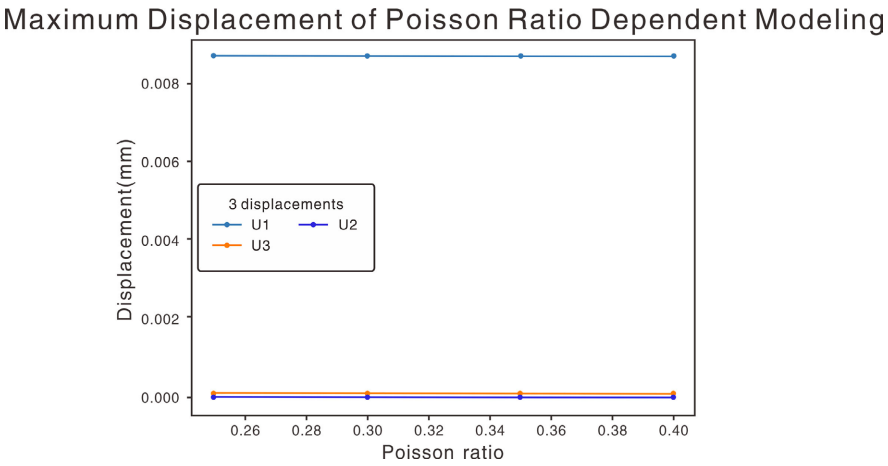

Figure 25. Maximum displacement of Poisson ratio dependent modeling.

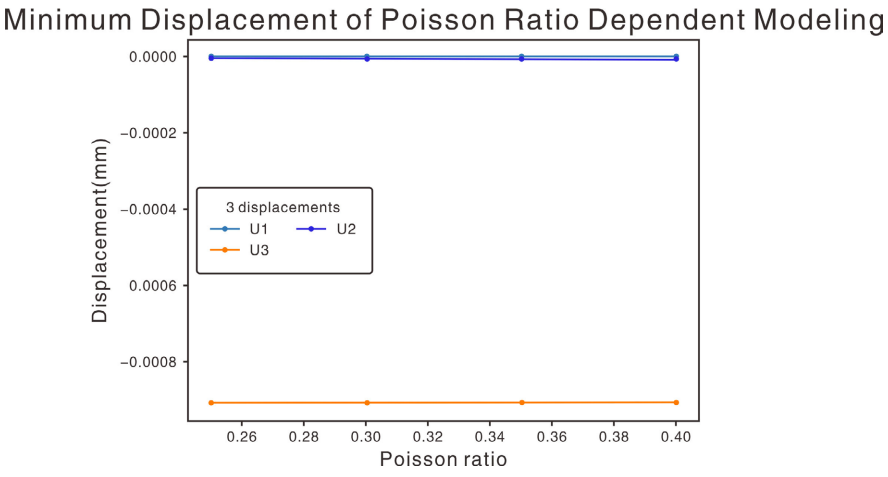

Figure 26. Minimum displacement of Poisson ratio dependent modeling.

Table 5. Displacement and stress.

U1max mm	U1min mm	U2max mm	U2min mm	U3max mm	U3min mm	S11max N/mm²	S11min N/mm²	S22max N/mm²	S22min N/mm²	S33max N/mm²	S33min N/mm²
8.70E−03	−4.80E−07	5.78E−06	−5.78E−06	9.69E−05	−9.07E−04	3.59E−03	−3.49E−03	1.91E−03	−3.12E−03	4.01E−03	−2.16E−02
8.70E−03	−6.80E−07	6.97E−06	−6.97E−06	9.69E−05	−9.06E−04	3.80E−03	−3.56E−03	2.19E−03	−3.87E−03	4.05E−03	−2.17E−02
8.69E−03	−8.94E−07	8.17E−06	−8.16E−06	9.69E−05	−9.06E−04	4.00E−03	−3.78E−03	2.54E−03	−4.68E−03	4.09E−03	−2.18E−02
8.68E−03	−1.12E−06	9.38E−06	−9.38E−06	9.69E−05	−9.05E−04	4.20E−03	−4.58E−03	2.89E−03	−5.53E−03	4.13E−03	−2.18E−02

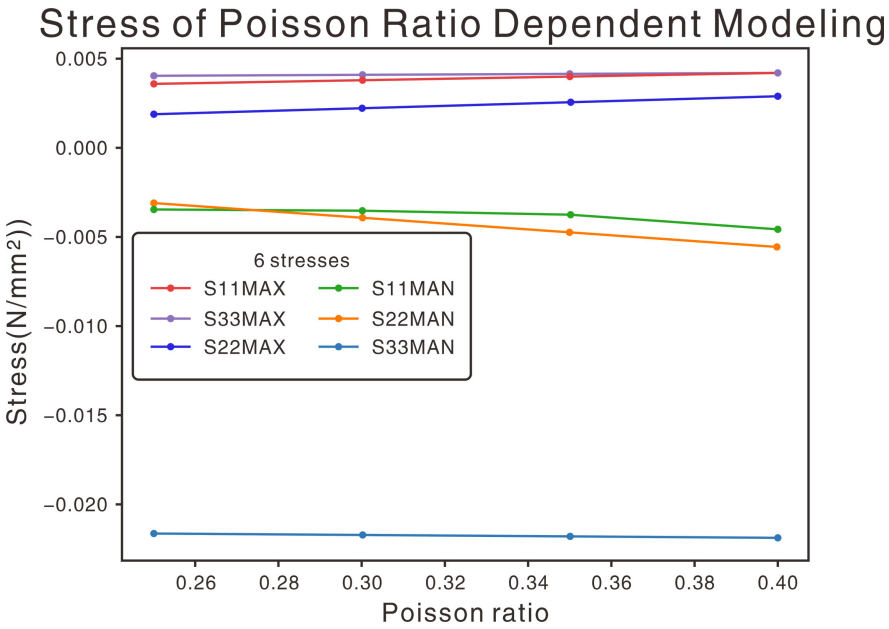

Figure 27. Max and min stress of Poisson ratio dependent modeling.

3.4. Loading of the Assembly

The roof of the factory is selected from the book *Prestressed concrete polylinear roof truss* [8]. According to the arrangement diagram, the roof is YWJ30-1. And steel structure is selected to compose the roof. The Table of roof truss technical and economic indicators is presented in Table 6. To simplify, a load of the same mass is applied to the top beam to simulate the real roof.

Since pure steel material is selected, the mass of the roof can be calculated multiplying the volume by the density of the steel, which is.

$$5.694\ m^3 \times 7850\ kg/m^3 = 44{,}698\ kg$$

This will give a load of 438,040 N to the beams that hold the roof. Considering the influence of weather factor, a snow pressure load is added to the total load of the factory.

The basic snow pressure shall be based on the 50-year reproduction period. So, we take 0.4 KN/m² in Beijing [9]. The projection of the roof on to the ground is 30 m × 66 m = 1980 m². Thus, the snow pressure is 1980 m² × 0.4 KN/m² = 792 KN. Combining of the loads gives the total load of the beams which is

1,230,040 N. 24 columns are holding the 2 beams, and each of the column will undertake 1/24 of the total loading which is 51,251 N. Due to the symmetry of the factory, the model is simplified into 5 columns in one side which is shown in Figure 28.

The load on each beam will still be 51,251 N, but it will not be directly applied to the top of the beam. Instead, the total load of the beam is 5/24 of the original load, which is 256,258 N will be applied to the surface of the top beam. The area of the beam is 400 mm × 33,100 = 13,240,000 mm^2. Switching the units into Newton per millimeter, the pressure will be. 0.01935 N/mm^2. A pressure of magnitude 0.088 N/mm^2 is applied to a small section of the surface of the crane rail in Figure 29, simulating the pressurization when the wheel of the crane is positioned at certain location of the crane rail.

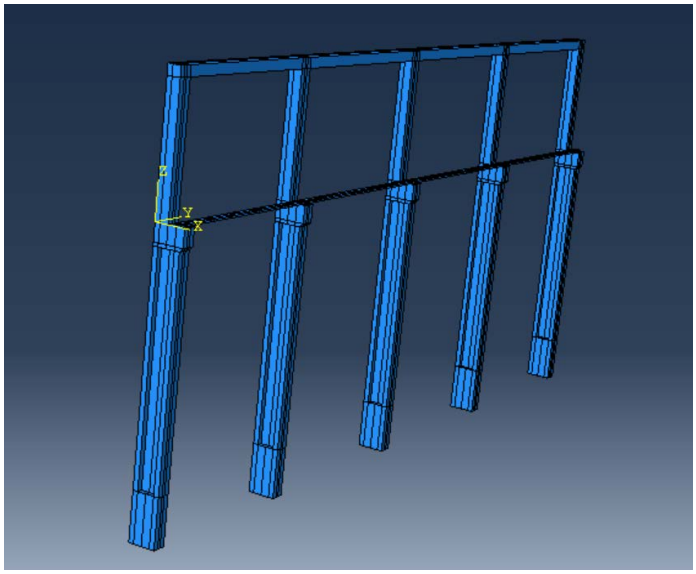

Figure 28. Simplified assembly of the factory.

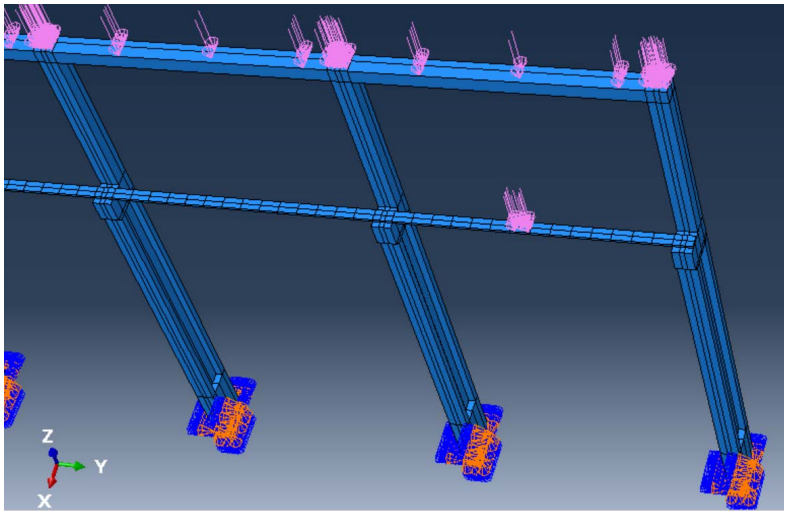

Figure 29. Location of different loadings.

The loading location in Figure 29 will result in a displacement of the rail which is shown in Figure 30. This figure is exaggerated as ABAQUS wants to show in the clear way where the displacement is happening.

The material properties of the steel are shown in the Table 7. And the loading is applied from one end to the other with a step size of one section in the Figure 30.

3.5. Loading Position Dependent Modeling

After running the job, data of displacement and stress is collected, and the concrete data points are plotted on Figure 31 to show the trend of displacement.

The U1 and U2, which stands for x and y direction, displacements are not so distinguishable. And Figure 32 is the zoomed in plot of them which provides a better indication of the trend.

The experimental results reveal sinusoidal-like trend lines, wherein the displacement exhibits a minimum value when the load is applied on the rail connected to the column, and a maximum value at the midpoint between two columns. These observations are consistent with the well-established principle that displacement is highest when the load is furthest from the supporting point. As the position changes, the stress also varies accordingly. Figure 33 displays a plot of stress versus position.

Table 6. Table of roof truss technical and economic indicators.

Roof truss type	Concrete volume (m^3)	Weight (t)	Steel		
			Weight (kg)		Total steel quantity (kg/m^3)
			prestressing steel	Normal steel	
YWJ30-1	5.694	14.235	204.79	932.67	199.76

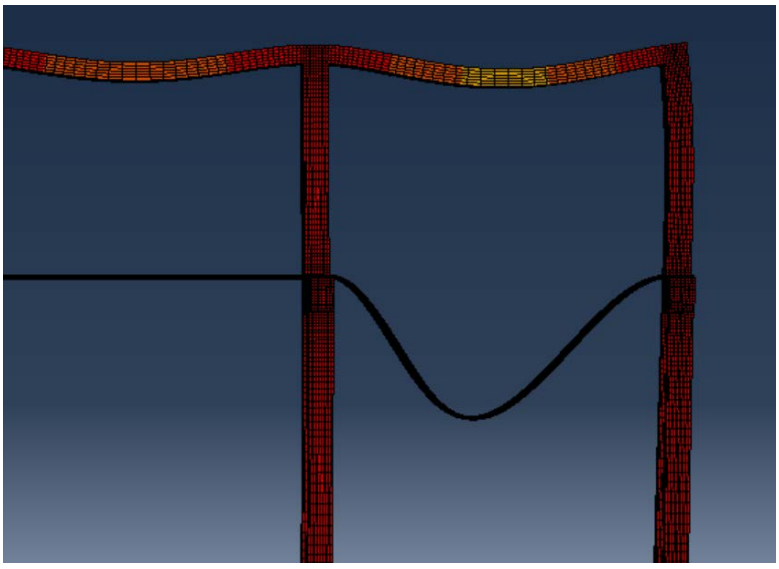

Figure 30. Visualization of displacement under loading.

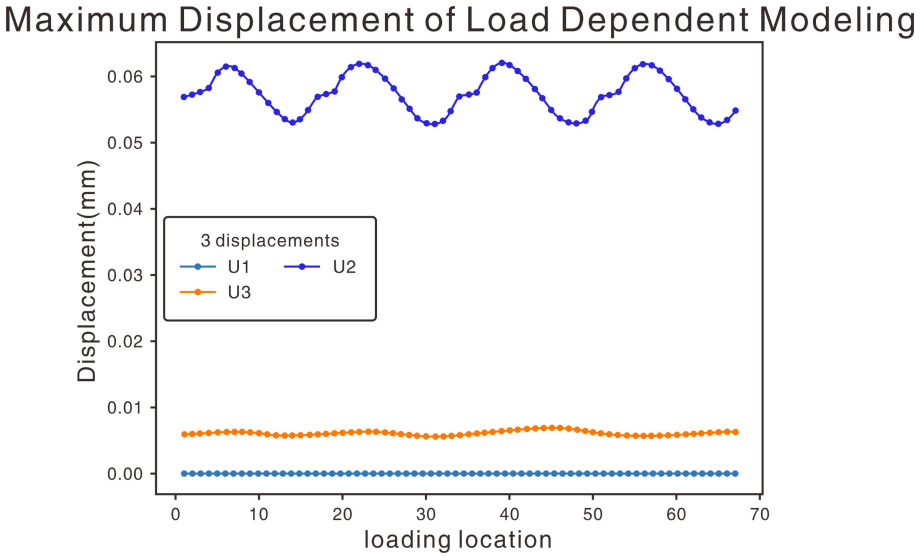

Figure 31. The maximum displacement versus loading location graph.

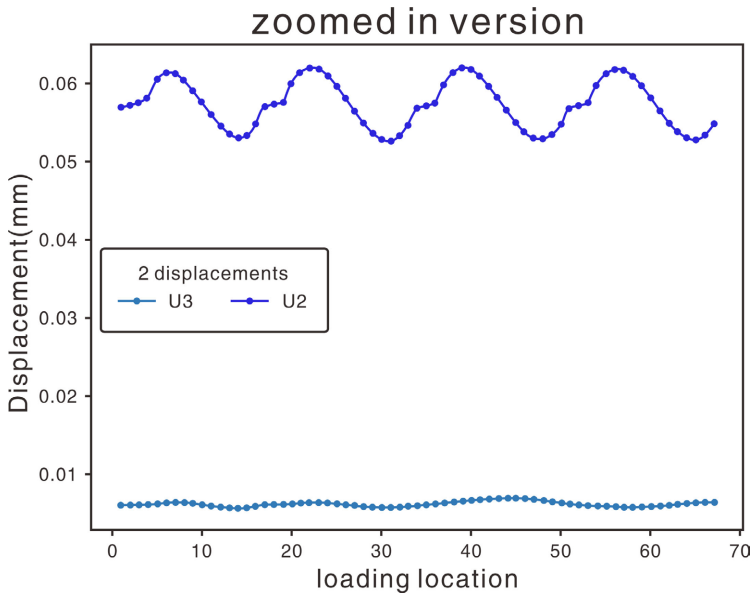

Figure 32. Zoomed in version of U2 and U3 displacements versus loading position.

Table 7. Material properties of the trail.

Young's modulus (N/mm)	Poisson's ratio	Density (kg/mm$^{3)}$
190,000	0.30	7.85×10^{-6}

The stress versus loading position plot presents a series of peaks, indicating that the stress is at its maximum between the columns. Furthermore, the flat section of the curve corresponds to the position on the column, which aligns with the established principle that displacement is at its highest when the load is farthest from the supporting point. As displacement and stress are positively correlated, the highest displacement corresponds to the highest stress, which is also reflected in the flat section of the curve.

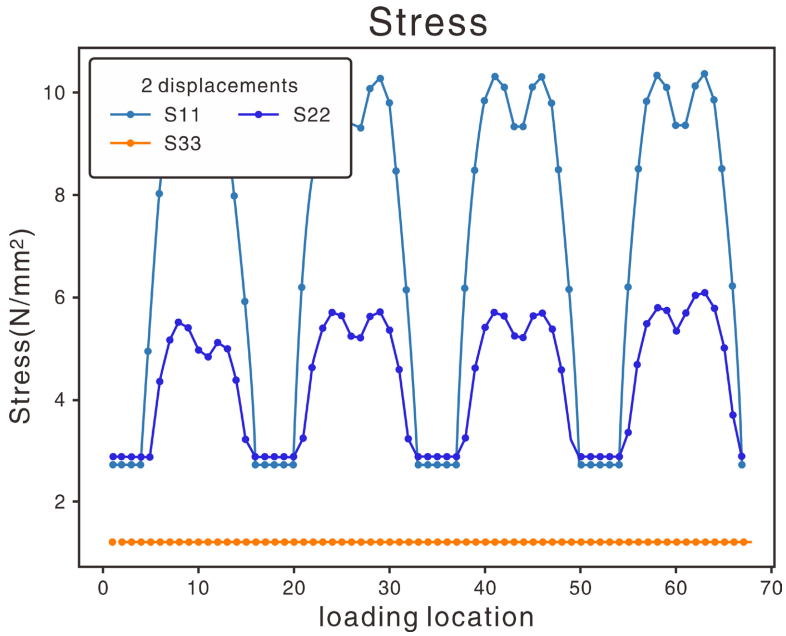

Figure 33. Stress versus loading location.

4. Conclusions

In conclusion, the displacement of a material in Abaqus is directly proportional to the load applied, with the stiffness of the material acting as the proportionality constant. This relationship between displacement and load is linear and can be expressed through the governing equations of elasticity. Young's modulus and Poisson's ratio are two key properties that affect the stiffness of a material and therefore play a crucial role in determining its ability to resist deformation under different types of loads. Increasing Young's modulus reduces the maximum displacement that occurs, while increasing Poisson's ratio results in a slight change in displacement and stress, with more stress occurring in the longitudinal direction. Overall, understanding the relationship between displacement, load, and material properties is important for accurately predicting and analyzing the behavior of structures under various loading conditions.

Furthermore, this relationship between load and displacement can be utilized to understand the behavior of a structure under different loading conditions. By analyzing the displacement of a structure under different loads, engineers can gain insight into its stiffness and its ability to withstand external forces. This information is crucial for designing structures that are both safe and efficient.

It is also important to note that the relationship between load and displacement is not always linear. In some cases, a structure may experience non-linear behavior due to material yielding or other factors. This non-linear behavior can cause the stiffness of the material to change, leading to a change in the relationship between load and displacement.

In conclusion, the relationship between load and displacement in Abaqus is governed by the elasticity equations and the stiffness of the material. By analyz-

ing the displacement of a structure under different loads, engineers can gain valuable insights into its behavior and design structures that are safe and efficient. However, it is important to consider non-linear behavior and other factors that may affect the relationship between load and displacement in some case.

Acknowledgements

I would like to express my sincere gratitude to my supervisor, Fei Yu, for providing me with valuable guidance, support, and encouragement throughout my research. Without his expertise and insights, this work would not have been possible. Finally, I would like to express my appreciation to my family and friends for their unwavering support and encouragement throughout my academic journey. Their love and encouragement have been a constant source of inspiration for me.

Conflicts of Interest

The author declares no conflicts of interest regarding the publication of this paper.

References

[1] Li, M. (2020) Study on Static and Dynamic Progressive Collapse of Shell Structures Based on Structural Response Sensitivity. Doctoral Dissertation, Southeast University, Nanjing.

[2] Peng, S. (2021) Performance Analysis and Key Technology Research on Large-Scale Industrial Buildings. Doctoral Dissertation, Tianjin University, Tianjin.

[3] Gao, X. (2019) Stability and Resistance to Progressive Collapse Analysis of Large-Span Single-Layer Cable-Supported Shell Structures. Doctoral Dissertation, Shandong University of Science and Technology, Qingdao.

[4] Ng, L.Y.A. and Wei, H.H. (2016) Effects of Connecting Plates on Cold-Formed Steel Wall Plate System. *Applied Mechanics and Materials*, **858**, 38-43. https://doi.org/10.4028/www.scientific.net/AMM.858.38

[5] Huang, C., Cui, J. and Long, L. (2003) Test and Analysis of Cold-Formed Thin-Walled C-Section Steel Beam-Column Joints Connected by Self-Tapping Screws. *Journal of Chongqing Jianzhu University*, **5**, 37-41.

[6] Huang, C. (2003) Experimental and Finite Element Analysis of Semi-Rigid Joints of Cold-Formed Thin-Walled C-Section Steel Beam-Columns. Doctoral Dissertation, Chongqing University, Chongqing.

[7] https://www.railwayrail.com/products/asce25-steel-rail/?lang=fr

[8] 04G415-1 Prestressed Concrete Polylinear Roof Truss. (n.d.).

[9] GB 50009-2012 (2012) Load Code for the Design of Building Structures. China Architecture & Building Press, Beijing.